ELSEVIER

Journal of Power Sources 56 (1995) 51–60

JOURNAL OF POWER SOURCES

Oxygen evolution and reduction on iridium oxide compounds

M.V. ten Kortenaar [a], J.F. Vente [a,1], D.J.W. IJdo [a,*], S. Müller [b], R. Kötz [b]

[a] *Leiden Institute of Chemistry, Gorlaeus Laboratories, Leiden University, PO Box 9502, 2300 RA Leiden, Netherlands*

[b] *Paul Scherrer Institute, 5232 Villigen, Switzerland*

Received 16 January 1995; revised 13 March 1995; accepted 15 March 1995

Abstract

The electrochemical properties of twelve iridium oxide compounds (including pyrochlores, perovskites, fluorites and compounds of another structure) were examined with respect to the oxygen-evolution and the oxygen-reduction reactions. Steady-state current–potential curves were measured in 45% KOH. In addition, the kinetic properties and the electrical conductivity of four iridium oxide pyrochlores were investigated. All twelve compounds have a moderate to high catalytic activity for the oxygen-evolution reaction, and a somewhat lower activity for the oxygen-reduction reaction. $Pb_2(Pb_xIr_{2-x})O_{7-y}$ and Nd_3IrO_7 showed the highest activity towards both reactions.

Keywords: Electrocatalysis; Pyrochlores; Iridium oxide compounds; Oxygen-evolution reaction; Electrical conductivity

1. Introduction

The motivation for the research on bifunctional oxygen electrocatalysts presented in this communication is their possible application in oxygen-evolving and reducing gas-diffusion electrodes for rechargeable metal/air batteries [1]. A fundamental problem of these battery systems is the limited lifetime of the bifunctional electrode. This problem has been traced to corrosion of the support material, e.g. carbon, and dissolution of the catalyst in the electrolyte [2]. Progress has been made in developing corrosion resistant carbon as the support for the bifunctional catalyst [3]. Promising activity and stability for the oxygen-evolution (OER) and -reduction reactions (ORR) in alkaline medium has been demonstrated for the pyrochlores $A_2B_2O_7$ with A = lead and/or bismuth and B = ruthenium or iridium [4–6]. In prototype secondary cells, especially, lead iridium oxide has been proven to be a good candidate material [7]. In addition, Swette et al. [5] have also investigated some (non-pyrochlore) iridium oxide compounds. Some mixtures of oxides appear to have a high activity towards the oxygen reactions. However, the research was not focused on pure compounds [5].

Several factors have been proposed to determine the performance of a compound in OER and ORR. Several authors [8–11] speculate about a relation between the catalytic activities and the density of states at the Fermi level. Shukla et al. [4] discuss the influence of the metal–oxygen binding energy and the π back bonding. The presence of oxygen vacancies, as observed in $Pb_2(Pb_xIr_{2-x})O_{7-y}$, has also been thought to be crucial in the electrocatalytic properties [8,12]. Other factors proposed are the electrical conductivity and the magnetic properties [11]. In most reaction mechanisms proposed for OER, the charge-transfer reaction is related to a specific surface redox couple [13].

Our attention will be focused on a model given by Goodenough et al. [12,14]. They proposed a reaction mechanism for ORR and one for OER on the pyrochlore $Pb_2(Pb_xIr_{2-x})O_{7-y}$ in an alkaline electrolyte. This is the only model proposed for an iridium oxide compound, and it may be a plausible reaction mechanism for other iridium oxide compounds as well. ORR is assumed to take place by a displacement of OH^- ions at oxygen sites, which are linked with lead. The oxygen of the Ir_2O_6 framework does not participate in this reaction. Oxygen evolution occurs at potentials anodic of the surface Ir^{4+}/Ir^{5+} couple [12,14]. In order to evolve oxygen at the catalyst the equilibrium $Ir^{4+}O^- \leftrightharpoons Ir^{5+}O^{2-}$ should not be biased to the right. This assumption could hold also for other compounds containing Ir^{4+}. A reaction mechanism with similar features is presented for $A_2Ru_2O_7$ with A = lead and bismuth [6]. Based on this reaction mechanism, a greater dependence on the A cation in $A_2Ir_2O_7$ is expected for ORR than for OER. Assuming that this model can be extended to other complex iridium(IV) oxide compounds, OER will occur on sites linked with iridium and ORR on sites linked with the other cation present. In Ir(V) compounds at

* Corresponding author.

[1] Present address: University of Oxford, Inorganic Chemistry Laboratory, South Parks Road, Oxford OX1 3QR, UK.

SSDI 0378-7753(95)02204-T

Table 1
Structural features and references of the catalysts studied

Catalyst	Structural features	Space group	Valency of Ir	Magnetic properties	Electrical conductivity [a]	Refs.
$Ln_2Ir_2O_7$ [b]	pyrochlore	$Fd\bar{3}m$	IV		see Table 5	[15], [19], [20]
$Pb_2(Pb_xIr_{2-x})O_{7-y}$	pyrochlore	$Fd\bar{3}m$	IV/V	TIP [c]	see Table 5	[4], [15], [20–23]
$Bi_2Ir_2O_7$	pyrochlore	$Fd\bar{3}m$	IV	Pauli	see Table 5	[15], [20]
Ln_3IrO_7 [b]	fluorite like	$Cmcm$	V	Curie–Weiss	≈ 2	[24], [25]
La_2MIrO_6 [d]	perovskite	$P2_1/n$	IV	Curie–Weiss	10^{-4}–10^{-2}	[26–29]
Sr_3CuIrO_6	Cu–Ir chains	$C2/c$	IV/V			[30]
$Ca_{4.73}Ir_3O_{12}$	Ca deficient	$P\bar{6}2m$	IV/V	Curie–Weiss		[31]
$(Sr/Pb)_2(Pb/Ir)_2O_7$	pyrochlore	$Fd\bar{3}m$	IV/V			[25]

[a] Electrical conductivity at room temperature in S cm^{-1}.
[b] Ln = Eu, Nd.
[c] TIP = temperature-independent paramagnetism, probably Pauli paramagnetism.
[d] M = Co, Ni, Zn.

oxidizing potentials, the equilibrium $Ir^{4+}O^- \leftrightharpoons Ir^{5+}O^{2-}$ is likely to be biased to the right. Formation of Ir^{6+} is not expected, since much higher potentials are usually required.

With the above-mentioned performance-determining factors in mind, we have selected some well-defined and crystallized iridium oxide compounds with a wide range of physicochemical properties. These compounds are summarized in Table 1, and their features are discussed below.

Four pure pyrochlore compounds were studied: $A_2Ir_2O_7$ with A = neodymium, europium, lead and bismuth. $Pb_2(Pb_xIr_{2-x})O_{7-y}$ was chosen as a reference material, since this is the only pure iridium oxide compound, which has been thoroughly investigated [4,5,7,12]. The fact that europium has a redox couple (Eu^{2+}/Eu^{3+}) within the potential range under investigation, while neodymium is trivalent only, could lead to different activities for ORR and/or OER. $Bi_2Ir_2O_7$ is known to be a metallic conductor [15] and, because of its high specific conductivity, an interesting candidate for the use as a bifunctional catalyst. Bismuth is expected to remain trivalent.

Two fluorite related compounds Nd_3IrO_7 and Eu_3IrO_7 were selected. In Ln_3IrO_7 iridium is found as Ir^{5+} only. These compounds can be compared with Ir^{4+} containing $Eu_2Ir_2O_7$ and $Nd_2Ir_2O_7$. In these compounds, oxygen bonded to the lanthanide is present on the surface. Based on Goodenough's model, similar trends towards the ORR in $Ln_2Ir_2O_7$ and Ln_3IrO_7 with Ln = europium and neodymium expected. The presence of Ir^{5+} is expected to slow down the OER as was discussed above.

Three ordered perovskites were chosen. Compounds with a perovskite-like structure, such as $(Ca/Sr/La)CoO_{3-y}$ [11,16–18] and $(Sr/La)MnO_{3-y}$ [11,17], are known to have a high catalytic activity. Both La_2CoIrO_6 and La_2NiIrO_6 were included because cobalt- and nickel-containing compounds can be active electrocatalysts [11] and both occur in di- and trivalent states. La_2ZnIrO_6 contains Zn^{2+}, which is not expected to contribute in the electrocatalytic activity. As can be seen in Table 1, the electrical conductivities of these ordered iridium-containing perovskites are low.

Three other compounds were taken for different reasons. Sr_3CuIrO_6 is one of the very few iridium oxide compounds containing copper [30]. Redox reactions may occur at both iridium and copper. $Ca_{4.73}Ir_3O_{12}$ is a recently prepared calcium-deficient compound [31]. Iridium is found as Ir^{4+} and as Ir^{5+}. The pyrochlore with two cations on the A-position $(Sr/Pb)_2(Pb/Ir)_2O_{7-y}$ was chosen to study the influence of the amount of lead on this position.

IrO_2 was not studied because of its worse oxygen-reduction performance compared with $Pb_2(Pb_xIr_{2-x})O_{7-y}$. The oxygen-evolution performance of these two compounds is comparable [5].

Steady-state current–potential curves were recorded for all compounds investigated. The pyrochlores $A_2Ir_2O_7$ (A = neodymium, europium, lead and bismuth) were studied more thoroughly. The galvanostatic measurements showed that these isomorphous compounds have a wide range of electrochemical activities towards OER and ORR. To study the influence of surface redox couples, the dynamic electrochemical properties (cyclic voltammetry) were examined. These electrochemical measurements were performed on Teflon-bonded electrodes. These electrodes are very similar to those that will be used in practical cells.

The electrical conductivity (four-probe on pressed pellets) of the pyrochlores investigated was measured, since the literature data were not consistent. The surface composition of $Pb_2(Pb_xIr_{2-x})O_{7-y}$ and the formal valences of lead and iridium in this compound were determined by X-ray photoelectron spectroscopy (XPS).

The goal of this work is to study the influence of the presence of several cations in pure iridium oxide compounds on the electrochemical activity towards OER and ORR. In addition, the influence of the formal oxidation state of iridium was studied.

2. Experimental

The twelve compounds were prepared by direct solid-state synthesis in air from stoichiometric mixtures of chemically

pure grade reactants, e.g. oxides and carbonates, and IrO_2, which was prepared as described by Vente and IJdo [24].

The samples $A_2Ir_2O_7$ (A = neodymium, europium) were prepared by firing first at 900 °C for three days and finally at 1000 °C for three days more.

$Bi_2Ir_2O_7$ was prepared by heating at 850 °C for eight days.

$Pb_2(Pb_xIr_{2-x})O_{7-y}$ was prepared by heating at 825 °C for two days. A decrease in mass of the reaction mixture was observed. X-ray diffraction (XRD) patterns revealed the presence of IrO_2. 10% excess of PbO was added, followed by a heat treatment at 825 °C for five days. This time, the XRD pattern did not show any impurities.

$(Sr/Pb)_2(Pb/Ir)_2O_{7-y}$ was prepared at 750 °C for two days. The target composition was $(Sr_{0.5}Pb_{1.5})$-$(Pb_{0.5}Ir_{1.5})O_{7-y}$. However, it is likely that, as during the preparation of $Pb_2(Pb_xIr_{2-x})O_{7-y}$, some PbO has evaporated. Sr_3CuIrO_6 was prepared at 800 °C for two days. The other catalysts were prepared as described in the literature, see Table 1.

All compounds prepared were examined for impurities by means of XRD in the range $10° < 2\theta < 90°$. The powder diffractometer used was a Philips PW 1050 powder diffractometer. The XRD patterns showed all the compounds to be single phased and highly crystalline. The XRD patterns are in agreement with the patterns reported in the literature.

The Teflon-bonded electrodes were prepared by mixing the catalyst and carbon (2:5 by weight) in a sufficient quantity of 2-propanol and water (1:1). The carbon used was Vulcan XC-72, fired at 2700 °C (Sigri, GmbH, Meitingen, Germany). The maximum particle size is approximately 125 μm, the specific surface area is about 70 $m^2\ g^{-1}$. A 60% Teflon (Du Pont) suspension was added and mixed thoroughly (catalyst:Teflon ratio 1:1.5). The paste was dried in air at 90 °C until the right consistency was achieved. The dry paste contains about 20% catalyst, 50% carbon and 30% Teflon. This paste was then mounted onto two sides of a silver gauze (diameter = 2.2 cm, degreased with acetone), and, subsequently, hot pressed at 320 °C and 50 kg cm^{-2} for 20 min. The prepared electrodes contain about 7 mg cm^{-2} catalyst, and are about 0.50 mm thick. The assembled test cell (Fig. 1), filled with 45% KOH, was left overnight in order to wet the gas diffusion electrode. All steady-state measurements were performed with oxygen supplied on the bottom of the working electrode. The current applied was accurate within 0.01 mA (for currents higher than 1 mA) or 1% (for currents lower than 1 mA). The geometrical surface area of the gas-diffusion electrodes was approximately 1.5 cm^2 (diameter = 0.7 cm). The potential was measured against a saturated sulfate (SSE) reference electrode (SSE, $E^0 = 662$ mV versus standard hydrogen electrode (SHE)) with an accuracy of 1 mV. The reproducibility of the measured potentials was better than 5 mV. During the measurements, the gas-side of the electrodes remained dry. The exact preparation route for the electrodes containing $A_2Ir_2O_7$ was slightly different from the route described above. For all compounds studied, one gas-diffusion electrode was prepared

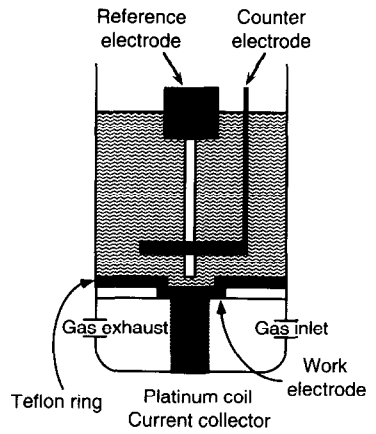

Fig. 1. A schematic drawing of the electrochemical cell used to test the bifuntional electrodes.

and its activity for the oxygen-reduction and -evolution reaction was compared with an electrode consisting of Teflon and graphitized carbon only (blank) and with an electrode containing $Pb_2(Pb_xIr_{2-x})O_{7-y}$.

Fig. 1 gives a schematic view of the experimental setup for the electrochemical measurements. A palladium ring served as the counter electrode. The working electrode was clamped between the cell and a platinum current collector. The steady-state current–potential curves were recorded using the galvanostatic mode of the potentiostat (Amel 555B), and were not corrected for ohmic potential drop. This is justified by the fact that the electrical resistivity of the electrodes used is mainly determined by the carbon and is the same for all electrodes. Cyclic voltammograms of the compounds $A_2Ir_2O_7$ were studied under oxygen, air and argon.

The electrical conductivity of the compounds $A_2Ir_2O_7$ was measured as a function of the temperature following the four-probe method as described by van der Pauw [32] between 30 and 800 °C. Pellets were prepared by pressing the powders at 200 kg cm^{-2} for 2 min, followed by sintering at 800 °C for one week. The pellets were connected with gold wires to the poles of a Solartron Schlumberger-1286 electrochemical interface.

The XPS pictures of $Pb_2(Pb_xIr_{2-x})O_{7-y}$ were measured on a Kratos ES 300 electron spectrometer using non-monochromatized Mg Kα radiation (1253.6 eV, 300 W). The fixed analyser transmission mode was chosen. The vacuum in the analysis chamber was always higher than 2×10^{-9} torr. The spectrum was recorded from a pressed pellet (about 1 mm thick). The pellet was mounted with a conductive paint to a platinum holder. The electron emission levels of Pb(4f), Ir(4f), O(1s) and C(1s) were recorded. Scattering cross sections for quantitative analysis were taken from [33]. No charging effects were observed.

3. Results and discussion

3.1. Galvanostatic measurements

The composition and dimensions of the electrodes are given in Table 2. This Table also gives the open-circuit poten-

Table 2
Electrode composition and specifications

Catalyst	Concentration (%)	Loading (mg cm^{-2})	d (mm)	E_{oc} (mV SSE)
$Nd_2Ir_2O_7$	≈24	≈6	≈0.5	−549
$Eu_2Ir_2O_7$	≈24	≈6	≈0.5	−525
$Pb_2(Pb_xIr_{2-x})O_{7-y}$	≈24	≈6	≈0.5	−504
$Bi_2Ir_2O_7$	≈24	≈6	≈0.5	−540
Nd_3IrO_7	23.0	7.6	0.55	−445
Eu_3IrO_7	21.2	6.2	0.40	−388
La_2CoIrO_6	20.3	6.5	0.43	−452
La_2NiIrO_6	20.3	5.3	0.40	−450
La_2ZnIrO_6	20.4	7.1	0.46	−511
Sr_3CuIrO_6	24.5	7.7	0.39	−490
$Ca_{4.73}Ir_3O_{12}$	20.6	8.6	0.54	−428
$(Sr/Pb)_2(Pb/Ir)_2O_7$	20.0	6.2	0.45	−560

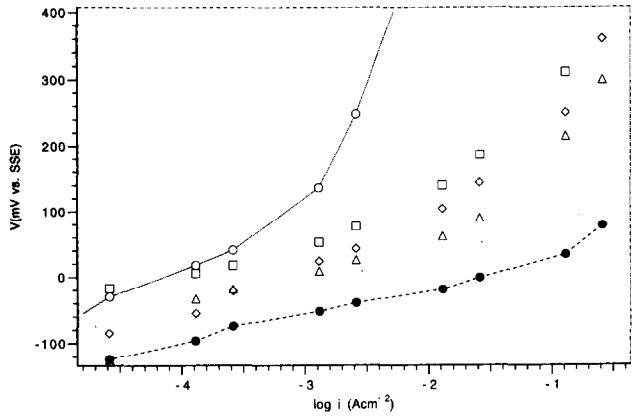

Fig. 2. Tafel plot of OER on $A_2Ir_2O_7$ with (◇) A = Nd, (△) A = Eu, (●) A = Pb, (□) A = Bi and (○) the blank.

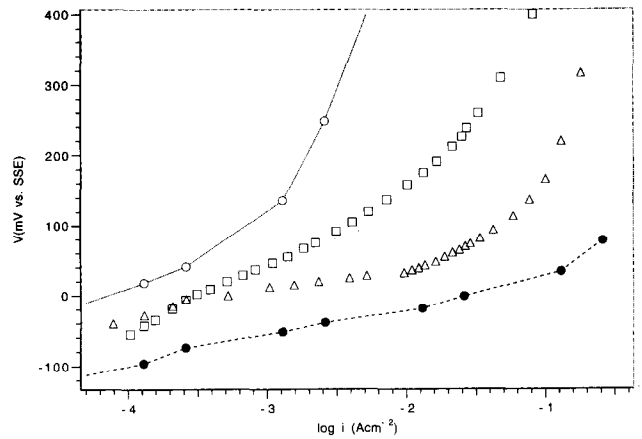

Fig. 3. Tafel plot of OER on Ln_3IrO_7 with (△) Ln = Nd and (□) Ln = Eu. The curves for (●) Pb–Ir pyrochlore and (○) the blank are given as reference.

tial (E_{oc}). Steady-state current–potential curves of the various catalysts for OER and ORR are given in Figs. 2–5 and 6–9, respectively. Tafel plots of $Pb_2(Pb_xIr_{2-x})O_{7-y}$ and of the blank are given for comparison. Tables 3 and 4 give the catalytic activity of the twelve compounds towards OER and ORR, respectively. In these Tables, the Tafel slope, the exchange-current density, the linear correlation coefficient (lcc) and the current densities, between which the Tafel equation is fitted, are presented. The low values for the lcc indicate that the Tafel curves are not straight curves. Consequently, the values of the Tafel slope tend to depend on the

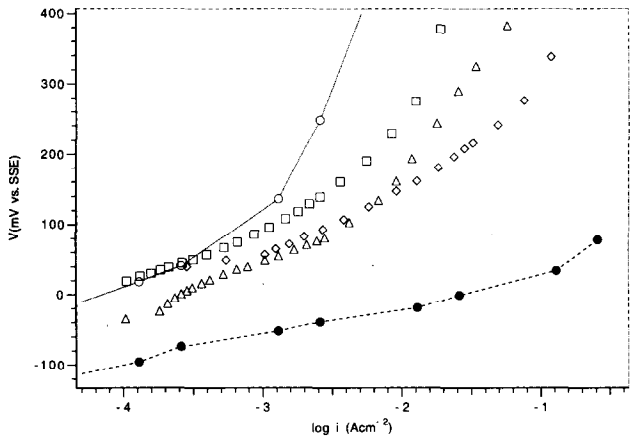

Fig. 4. Tafel plot of OER on La_2MIrO_6 with (△) M = Co, (◇) M = Ni and (□) M = Zn. The curves for (●) Pb–Ir pyrochlore and (○) the blank are given as reference.

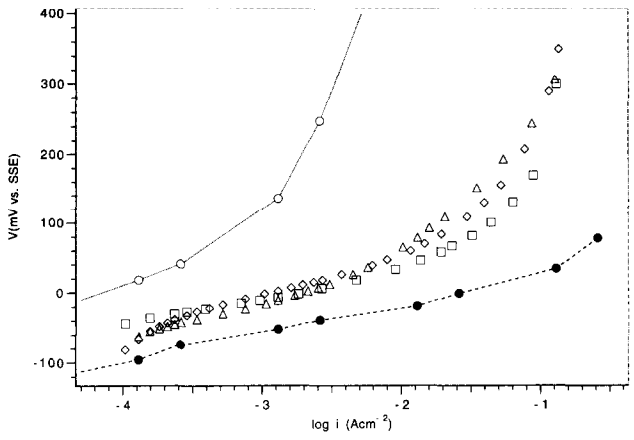

Fig. 5. Tafel plot of OER on (□) Sr–Pb–Ir pyrochlore, (△) $Ca_{4.73}Ir_3O_{12}$ and (◇) Sr_3CuIrO_6. The curves for (●) Pb–Ir pyrochlore and (○) the blank are given as reference.

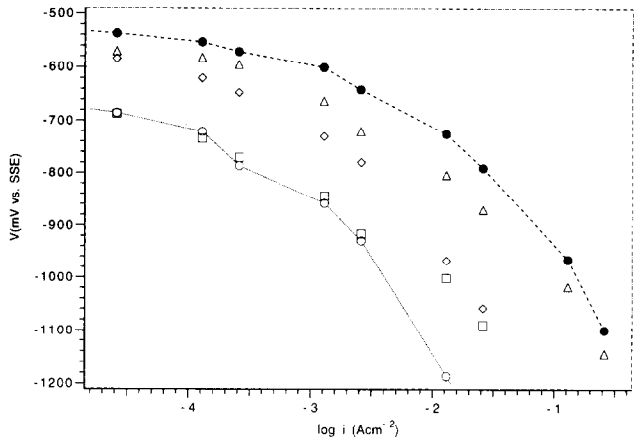

Fig. 6. Tafel plot of ORR on $A_2Ir_2O_7$ with (◇) A = Nd, (△) A = Eu, (●) A = Pb, (□) A = Bi and (○) the blank.

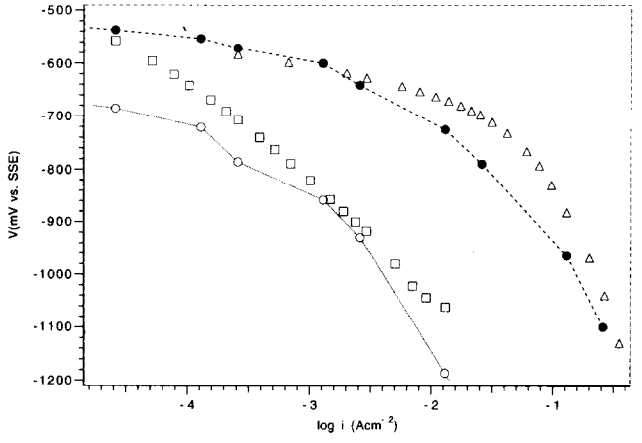

Fig. 7. Tafel plot of ORR on Ln_3IrO_7 with (△) Ln = Nd and (□) Ln = Eu. The curves for (●) Pb–Ir pyrochlore and (○) the blank are given as reference.

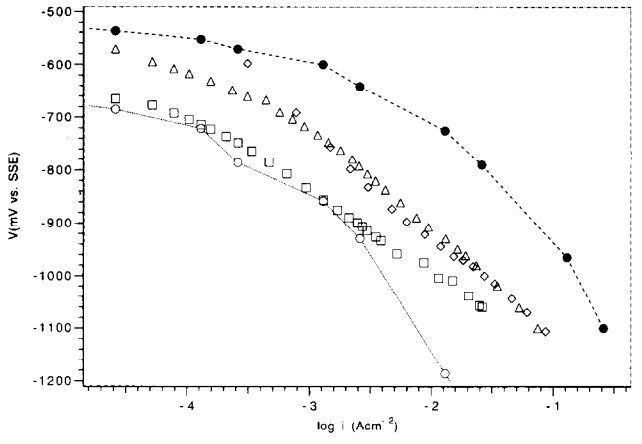

Fig. 8. Tafel plot of ORR on La_2MIrO_6 with (△) M = Co, (◇) M = Ni and (□) M = Zn (squares). The curves for (●) Pb–Ir pyrochlore and (○) the blank are given as reference.

current density range used in the fit. For these reasons also the potentials (versus SSE) at the current densities 1 and 10 mA cm^{-2} are given (Tables 3 and 4). The open-circuit potential for the compounds studied ranges from −560 mV versus SSE ($(Sr/Pb)_2(Pb_xIr_{2-x})O_{7-y}$) to −388 mV versus SSE (Eu_3IrO_7).

The twelve compounds are more effective catalysts in OER than they are in ORR. For both reactions, the overpotential is fairly high. The active surface area appears to be the primary factor affecting the performance of the electrodes. High surface area carbon instead of graphitized carbon (70 m^2 g^{-1}) and compounds prepared by a low-temperature synthesis route with BET surface area greater than 50 m^2 g^{-1} would markedly improve the OER and ORR activity [21].

In agreement with our expectations ORR depends on the other cation present more strongly than does OER. The differences in catalytic activity towards ORR between the catalysts and carbon are much smaller than in case of OER. Still, the differences between the several catalysts are substantial.

The observed polarization curves are dependent on the microstructure of our gas-diffusion electrodes. However, with the highly standarized preparation procedure of the electrodes we have tried to minimize the difference in microstructure of the electrodes. So, the differences in the polarization curves will be mainly due to differences in electrocatalytic activities of the catalysts. Below, the electrochemical properties of the twelve compounds are discussed in more detail.

3.2. Oxygen-evolution reaction

All compounds investigated are moderately to highly active for OER with Tafel slopes ranging from 25 to 114 mV dec^{-1} (Table 3). The semi-logarithmic polarization curves measured for OER show more or less linear shape up to about 20 mA cm^{-2} for all catalysed electrodes. At current densities higher than 100 mA cm^{-2}, the active surface of the electrodes was partially covered by oxygen bubbles and the potentials measured versus the reference electrode were not reproducible.

The pyrochlore with the highest activity is the reference compound $Pb_2(Pb_xIr_{2-x})O_{7-y}$ (Fig. 2). The overpotential

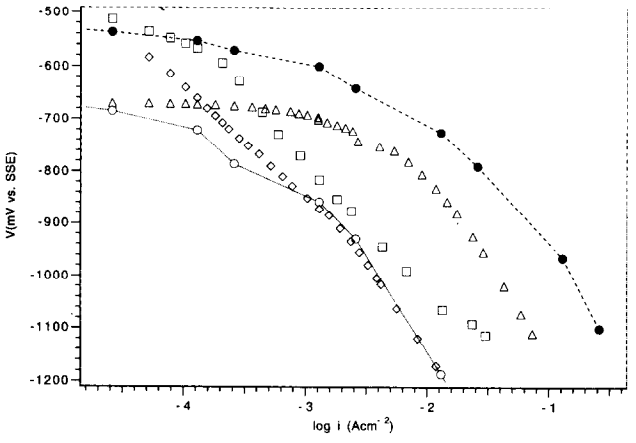

Fig. 9. Tafel plot of ORR on (□) Sr–Pb–Ir pyrochlore, (△) $Ca_{4.73}Ir_3O_{12}$ and (◇) Sr_3CuIrO_6. The curves for (●) Pb–Ir pyrochlore and (○) the blank are given as reference.

Table 3
Results of oxygen-evolution reactions

Catalyst	Slope (mV dec^{-1})	i_0 (mA cm^{-2})	lcc [a]	Fit region (mA cm^{-2})		1 mA [b] (mV SSE)	10 mA [b] (mV SSE)
$Nd_2Ir_2O_7$	76(4)	3.6×10^{-8}	0.996	0.13	13	13	92
$Eu_2Ir_2O_7$	51(3)	3.3×10^{-11}	0.993	0.13	25	2	58
$Pb_2(Pb_xIr_{2-x})O_{7-y}$	38(2)	1.5×10^{-12}	0.992	0.13	25	−58	−20
$Bi_2Ir_2O_7$	65(7)	1.9×10^{-10}	0.985	0.13	13	45	130
Nd_3IrO_7	25(1)	1.5×10^{-18}	0.994	0.26	12.02	11	33
Eu_3IrO_7	114(4)	1.6×10^{-4}	0.992	0.38	21.88	44	154
La_2CoIrO_6	95(2)	4.7×10^{-6}	0.998	1.04	12.88	56	150
La_2NiIrO_6	78(2)	4.4×10^{-7}	0.995	0.20	2.81	47	172
La_2ZnIrO_6	88(3)	1.2×10^{-7}	0.991	0.10	3.63	92	247
Sr_3CuIrO_6	57(1)	2.8×10^{-9}	0.997	0.18	14.79	−3	55
$Ca_{4.73}Ir_3O_{12}$	52(2)	3.3×10^{-11}	0.994	0.18	4.57	−17	64
$(Sr/Pb)_2(Pb/Ir)_2O_7$	47(3)	1.2×10^{-9}	0.991	0.23	23.44	−11	36

[a] Linear correlation coefficient.
[b] Potential at 1 and 10 mA cm^{-2}, respectively.

remains low up to about 100 mA cm^{-2}. The Tafel slope of 38 mV dec^{-1} agrees reasonably well with the literature data of 60 mV dec^{-1} [12] and 30 mV dec^{-1} [4,7]. The latter value was determined on pressed pellets, which did not contain carbon. $Eu_2Ir_2O_7$ has also a good performance. The activity of $Bi_2Ir_2O_7$ is remarkably low.

On basis of the reaction mechanism proposed by Goodenough et al. [12,14] one may expect that Ir(V)-containing compounds have a low activity. Indeed, this is found for Eu_3IrO_7. This compound has the highest Tafel slope of all compounds investigated (114 mV dec^{-1}). However, Nd_3IrO_7 is a good catalyst in OER with a very low Tafel slope up to rather high current densities. Only at $i \approx 100$ mA cm^{-2}, the polarization starts to increase rapidly due to the formation of oxygen bubbles on the active surface (Fig. 3). Apparently, the reaction mechanism of oxygen evolution on Nd_3IrO_7 does not conform to Goodenough's model.

As shown in Fig. 4, the perovskite-like compounds have a moderate Tafel slope in OER. The potentials at 1 and 10 mA cm^{-2} are rather high. As expected, the perovskite with the lowest activity is La_2ZnIrO_6. The Tafel plot of La_2CoIrO_6 is linear up to about 12 mA cm^{-2}, almost a decade higher than the other two perovskites.

The performance of the three remaining compounds is rather good (Fig. 5). The difference between the activity of $(Sr/Pb)_2(Pb_xIr_{2-x})O_{7-y}$ and of $Pb_2(Pb_xIr_{2-x})O_{7-y}$ is rather small. This is in agreement with our expectation that the A cation has a stronger influence on ORR than on OER. It may also be the case that the addition of strontium does not alter the surface composition, which contains more lead than the stoichiometry (see the results of the XPS measurements). The electrochemical properties of $Ca_{4.73}Ir_3O_{12}$ and Sr_3CuIrO_6 are similar. The activity of the compound with the lowest iridium content, Sr_3CuIrO_6, may be connected with a changing electron configuration as $Cu^{2+}Ir^{4+}/Cu^{+}Ir^{5+}$. The compound $Ca_{4.73}Ir_3O_{12}$ is a mixed valence compound (Ir^{4+}/Ir^{5+}) and is calcium deficient.

3.3. Oxygen-reduction reaction

The twelve compounds have a low to moderate activity in ORR with Tafel slopes ranging from −61 to −327 mV dec^{-1}. Above 25 mA cm^{-2} the overpotential starts to rise quickly. Oxygen-diffusion hindrance in the porous electrode is the dominant parameter for this increasing polarization.

A Tafel slope of 61 mV dec^{-1} calculated for the kinetically controlled low current region was obtained with $Pb_2(Pb_xIr_{2-x})O_{7-y}$. Tafel slopes of 60 mV dec^{-1} [12] and 55 mV dec^{-1} [4,7] have been reported for this compound. However, the latter value was determined on pressed pellets, which did not contain carbon. As depicted in Fig. 6, a good performance for ORR was also observed for $Eu_2Ir_2O_7$. At 1 mA cm^{-2} the difference in polarization is about 55 mV between the lead and europium pyrochlores. Compared with a pure carbon electrode (blank) the reduction potential could be improved by 200 mV. Significantly higher polarization was measured for the neodymium and bismuth pyrochlores. For currents up to 1 mA cm^{-2} the current–potential curve for the neodymium-catalysed electrode is about 100 mV more positive than that for the bismuth-catalysed electrode. At higher current densities the increase in overpotential may be due to the low conductivity of the neodymium catalyst (Table 5). For this electrode, oxygen-reduction potentials are between 10 and 100 mA cm^{-2}, comparable with those obtained from the blank.

As shown in Fig. 7, the highest performance is observed for Nd_3IrO_7; it is even somewhat better than that of $Pb_2(Pb_xIr_{2-x})O_{7-y}$. In contrast to Nd_3IrO_7, Eu_3IrO_7 does not exhibit a high activity for oxygen reduction. This is a remarkable result especially since oxygen is much more easily reduced on $Eu_2Ir_2O_7$ than on $Nd_2Ir_2O_7$.

ORR at perovskite-like compounds shows the same tendency as OER. La_2ZnIrO_6 has a lower activity than the other two (Fig. 8).

Table 4
Results of oxygen-reduction reactions

Catalyst	Slope (mV dec^{-1})	i_0 (mA cm^{-2})	lcc [a]	Fit region (mA cm^{-2})		1 mA [b] (mV SSE)	10 mA [b] (mV SSE)
$Nd_2Ir_2O_7$	−121(8)	6.8×10^{-2}	0.972	0.13	2.6	−712	−930
$Eu_2Ir_2O_7$	−124(9)	6.2×10^{-2}	0.988	0.13	26.0	−650	−787
$Pb_2(Pb_xIr_{2-x})O_{7-y}$	−61(7)	2.3×10^{-2}	0.980	0.13	2.6	−595	−709
$Bi_2Ir_2O_7$	−149(9)	8.5×10^{-3}	0.990	0.13	26.0	−829	−985
Nd_3IrO_7	−63(4)	8.5×10^{-3}	0.993	2.04	25.12	−605	−660
Eu_3IrO_7	−186(3)	4.5×10^{-3}	0.998	0.05	2.95	−820	−1049
La_2CoIrO_6	−198(4)	4.2×10^{-2}	0.996	0.30	87.10	−716	−930
La_2NiIrO_6	−92(4)	1.5×10^{-3}	0.994	0.02	0.91	−723	−911
La_2ZnIrO_6	−151(2)	6.5×10^{-3}	0.998	0.10	5.24	−838	−990
Sr_3CuIrO_6	−221(3)	2.2×10^{-2}	0.997	0.05	4.26	−848	−1145
$Ca_{4.73}Ir_3O_{12}$	−327(9)	1.7×10^{0}	0.995	7.07	74.13	−692	−815
$(Sr/Pb)_2(Pb/Ir)_2O_7$	−243(6)	3.7×10^{-2}	0.996	0.20	30.20	−783	−1032

[a] Linear correlation coefficient.
[b] Potential at 1 and 10 mA cm^{-2}, respectively.

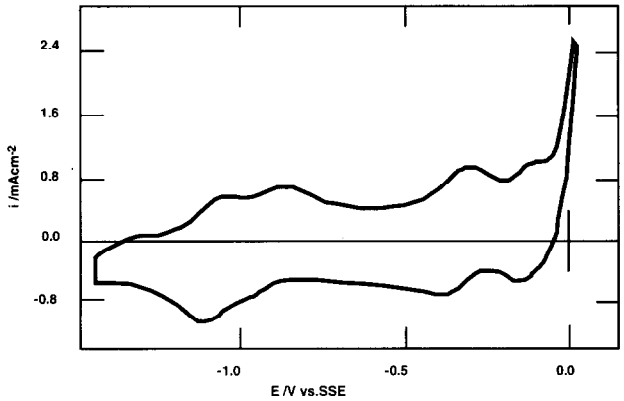

Fig. 10. Cyclic voltammogram for $Pb_2(Pb_xIr_{2-x})O_{7-y}$ in 45% KOH; scan rate = 100 mV s^{-1}.

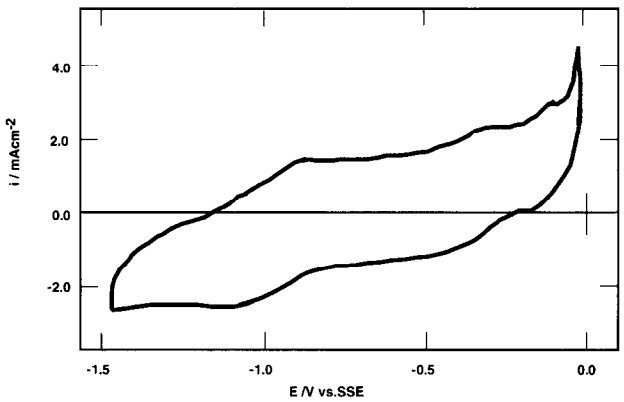

Fig. 11. Cyclic voltammogram for $Eu_2Ir_2O_7$ in 45% KOH; scan rate = 100 mV s^{-1}.

The three remaining compounds have a low to moderate activity for ORR (Fig. 9). Only the performance of $Ca_{4.73}Ir_3O_{12}$ is significantly better than the blank. The activity of $(Sr/Pb)_2(Pb_xIr_{2-x})O_{7-y}$ is considerably lower than the performance of $Pb_2(Pb_xIr_{2-x})O_{7-y}$. Such a large effect is in agreement with the assumption that ORR takes place on the oxygen positions linked with the A cation in $A_2Ir_2O_7$.

3.4. Dynamic measurements

The voltammogram of $Pb_2(Pb_xIr_{2-x})O_{7-y}$ under argon flow, presented in Fig. 10, shows a couple of quasi-reversible peaks. The cyclic voltammograms (CVs) reported in the literature, measured on pressed pellets with up to 16 wt.% Teflon in air, are rather featureless and the only major peaks observed are due to oxygen reduction and evolution [4,7,12]. The double-layer capacity of these electrodes is high. The CV presented in Fig. 10 shows a small capacitive current and clearly visible peaks. The small capacity is characteristic for this type of electrode [34]. The peak at −330 mV is the Ir^{4+}/Ir^{5+} couple [12]. One of the double-shaped quasi-reversible peaks between −850 and −1100 mV is due to the Ir^{3+}/Ir^{4+} couple [12]. The source of the other peak is unknown. It is not observed under an oxygen or under an air stream. In that case, the signal for ORR is strongly favoured over the signal for redox transitions of the catalyst. The strong quasi-reversible peaks are located just at the potential where the onset of ORR in air and oxygen occurs. Finally, the quasi-reversible peak at −130 mV can be ascribed to the Pb^{2+}/Pb^{4+} transition [35,36].

The CV of $Eu_2Ir_2O_7$, as shown in Fig. 11, has smaller peaks at similar potentials compared with the CV of $Pb_2(Pb_xIr_{2-x})O_{7-y}$. The peaks may correspond to similar redox transitions as in $Pb_2(Pb_xIr_{2-x})O_{7-y}$. The Ir^{3+}/Ir^{4+}, Ir^{4+}/Ir^{5+} and Eu^{2+}/Eu^{3+} transitions are visible.

Fig. 12 shows the CV of $Bi_2Ir_2O_7$. The double peak is again found at about −1000 mV. However, its intensity and shape are very different. The potential of the peak resulting from the Ir^{4+}/Ir^{5+} is slightly more positive than that of $Pb_2(Pb_xIr_{2-x})O_{7-y}$ and $Eu_2Ir_2O_7$.

The CV of $Nd_2Ir_2O_7$ (see Fig. 13) does not show any major peaks. The cathodic part of the CV of $Bi_2Ir_2O_7$

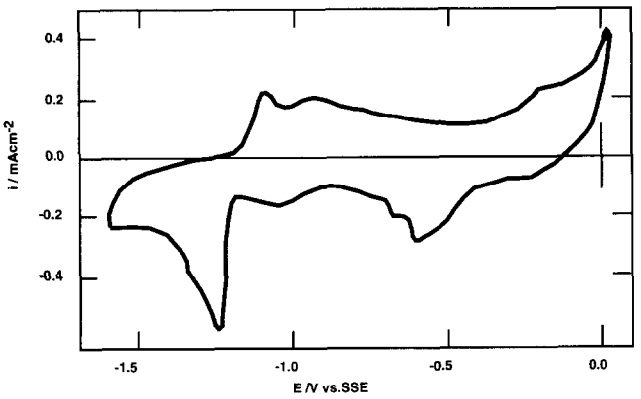

Fig. 12. Cyclic voltammogram for $Bi_2Ir_2O_7$ in 45% KOH; scan rate = 100 mV s^{-1}.

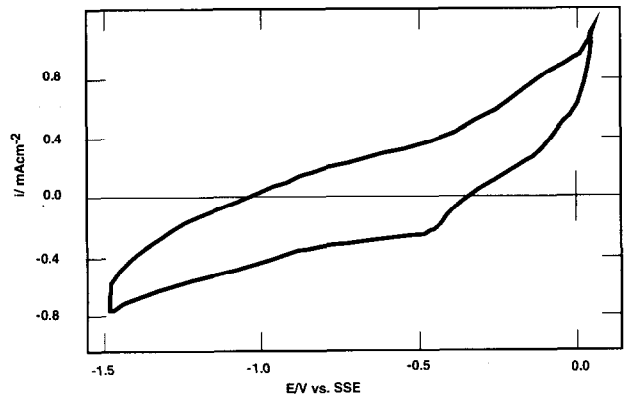

Fig. 13. Cyclic voltammogram for $Nd_2Ir_2O_7$ in 45% KOH; scan rate = 100 mV s^{-1}.

and, to a lesser extent, $Nd_2Ir_2O_7$ shows some irreversible peaks.

The two compounds with the highest activity towards OER show both quasi-reversible peaks just before the onset of oxygen evolution. This is also observed by Wattiaux [37]. These peaks can be ascribed to the following redox couples: Ir^{4+}/Ir^{5+}, Pb^{2+}/Pb^{4+} or Eu^{2+}/Eu^{3+}. Thus, a transition of the A cation seems to improve the catalytic activity towards OER. Bismuth and neodymium were not expected to show any transition, and none was observed.

As discussed in Section 3.3, reducing pyrochlores will give differences in the CVs of the various pyrochlores. The CVs do show major differences in the occurrence, the potential and the intensity of the peaks below −750 mV versus SSE. However, this potential region shows some non-interpretable peaks. The role of these peaks in the catalytic properties towards ORR is unclear.

3.5. Electrical conductivity

Fig. 14 shows the electrical conductivity $A_2Ir_2O_7$ with A = neodymium, europium, lead and bismuth as a function of the temperature studied. The compounds with a positive temperature gradient have been fitted to an Arrhenius-type

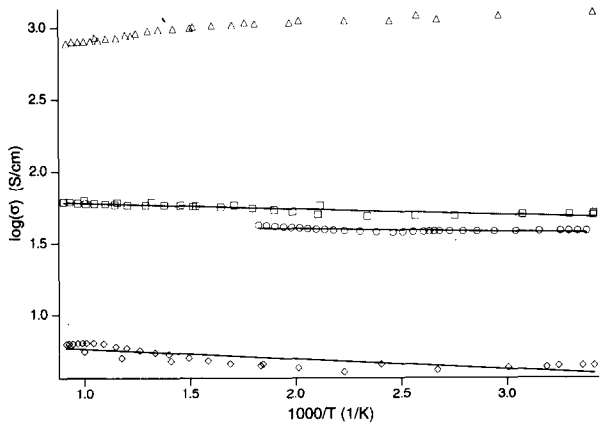

Fig. 14. Electrical conductivity of $A_2Ir_2O_7$ with (◇) A = Nd, (△) A = Eu, (○) A = Pb and (□) A = Bi vs. temperature.

Table 5
The electrical conductivity of the four pyrochlores studied at 30 °C

Compound	$\sigma_{30\,°C}$ (S cm^{-1})			E_a (eV)
	Ref. [15]	Ref. [38]	Our data	
$Nd_2Ir_2O_7$		200	4.5(5)	0.05(2)
$Eu_2Ir_2O_7$	40	170	38(4)	0.018(4)
$Pb_2(Pb_xIr_{2-x})O_{7-y}$		4500	50(4)	0.035(2)
$Bi_2Ir_2O_7$	1000	120	1220(76)	

relation. In Table 5, the activation energy and the specific conductivity at 30 °C are given. This Table also gives a comparison with earlier reported values. The conductivity ratio of $Bi_2Ir_2O_7$ at 30 and 700 °C, as a measure for the metallicity of this compound, is 1.6. The specific conductivity of the four pyrochlores is almost independent of the temperature. Except for $Bi_2Ir_2O_7$, these compounds have a small, though distinctly positive temperature coefficient. Our data fit well with the results of Bouchard and Gillson [15], but are not comparable with the data presented by Lazarev and Shaplygin [38].

In analogy with the conductivity mechanism for $SrRuO_3$ [39], the electrical conductivity of pyrochlores $A_2B_2O_7$ is believed to be due to the formation of a B–O conduction band [15,40]. The width of this band and the splitting (probably of the Mott–Hubbard type) of the B–O states are suggested to depend on the A ion. A post-transition element (as bismuth or lead) on the A position results in a broad band, while a lanthanide results in a much narrower band. This can be ascribed to the presence of empty s orbitals of bismuth or lead in the same energy range as the d band. The remarkably low conductivity and the negative temperature coefficient of the lead pyrochlore is ascribed to the incorporation of lead as Pb^{4+} at the B position. Pb^{4+} has no electrons to give up to the conduction band; a break in the –B–O–B–O–B– pathway occurs, resulting in a decrease of the electrical conductivity. The possible presence of some amorphous lead oxide in the sample would also result in a decreasing conductivity.

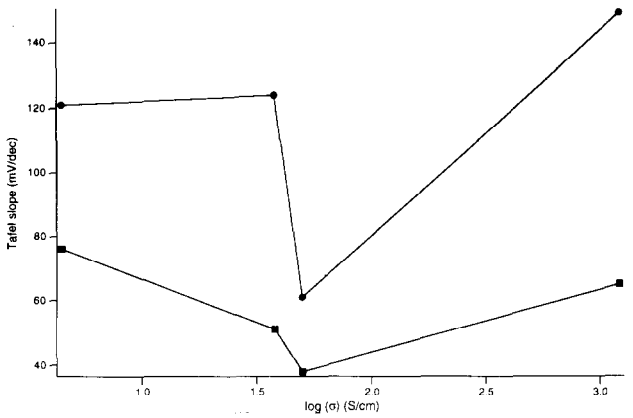

Fig. 15. Tafel slope of the four pyrochlores investigated for (●) OER and (■) ORR vs. specific conductivity.

The specific conductivity of $Eu_2Ir_2O_7$ is about an order of magnitude higher than the specific conductivity of $Nd_2Ir_2O_7$. This may connected with a changing electron configuration from $Eu^{3+}Ir^{4+}$ to $Eu^{2+}Ir^{5+}$, providing an additional possible pathway for the conduction. Such an electron configuration is also used to interpret the CV of $Eu_2Ir_2O_7$.

Fig. 15 shows the measured Tafel slopes of the four pyrochlores as a function of the specific conductivity. No enhanced activity for both OER and ORR with increasing conductivity is observed.

3.6. X-ray photoelectron spectroscopy

Performing XPS measurements on $Pb_2(Pb_xIr_{2-x})O_{7-y}$ was justified by the fact that PbO evaporation was observed during its preparation. The binding energies of the Ir(4f) and O(1s) levels in $Pb_2(Pb_xIr_{2-x})O_{7-y}$, determined with XPS, are 61.6 and 529.6 eV, respectively. The lead level indicated two lead surface species with binding energies of 137.3 and 138.7 eV, respectively. The lead and iridium binding energies clearly indicate that the metal is in its oxidized state. While the position of the iridium level can be attributed to Ir(IV) [41,42], the chemical shift of the lead level indicates the presence of Pb(II) and Pb(IV) [43]. The position of the O(1s) level is typical for oxygen in metal oxides. The Pb:Ir:O ratio at the surface was found to be 2.1:1:7,indicating an excess of lead oxide. Preliminary results of energy dispersion X-ray measurements on several samples prepared with different Pb:Ir ratios indicate that the composition of formed crystals is almost constant and independent of the overall Pb:Ir ratio. Enrichment of the surface with lead has been observed by Gökagaç and Kennedy [44] for $Pb_2(Pb_xRu_{2-x})O_{7-y}$. The high Pb:Ir ratio is likely to be due to the formation of some amorphous lead oxide (probably PbO_2 [44]) in the bulk and a further enrichment of the surface.

It has to be noticed that carbon was found in significant amounts (20%). The presence of lead oxide on the surface is not sufficient to explain the excess amount of oxygen. Therefore it is assumed, that some oxygen originates from carbon or water contamination. No depth profile could be constructed due to sputtering-induced reduction as observed on IrO_2 and PbO [45].

4. Conclusions

The compounds $Pb_2(Pb_xIr_{2-x})O_{7-y}$ and Nd_3IrO_7 have the highest activity for both OER and ORR. These compounds are good candidates for bifunctional catalysts.

The difference in catalytic properties of the pyrochlores examined here presumably correlates with presence of a redox transition of the A cation at about -150 mV versus SSE. However, the high activity of $Pb_2(Pb_xIr_{2-x})O_{7-y}$ may also be ascribed to the influence of oxygen deficiency.

The catalytic activity of the pyrochlores towards ORR studied tends to be more dependent on the A cation than the catalytic activity towards OER. This is in agreement with the mechanisms proposed by Goodenough et al. [12,14] which assume that the oxygen reduction takes place via displacement of OH^- ions at the oxygen sites which are linked with lead, and oxygen evolution occurs at potentials anodic to the surface Ir^{4+}/Ir^{5+} couple [12,14].

Our results do not reveal any possible correlation between the electrochemical and the electronic properties.

Acknowledgements

This work was financially supported by the Swiss Federal Energy Office. The authors are grateful to Professor Dr J.A.R. van Veen for his comments on this manuscript and to Dr B. Schyder, Paul Scherrer Institute, for performing XPS measurements; they are also grateful to Magneto Chemie, Schiedam, The Netherlands, for supplying chloroiridic acid, and to TNO, Eindhoven, The Netherlands, for the electrical conductivity measurements.

References

[1] S. Müller, K. Stiebel and O. Haas, *Electrochim. Acta, 39* (1994) 1661.
[2] C. Fierro, R.E. Carbonio, D. Scherson and E.B. Yeager, *Electrochim. Acta, 33* (1988) 941.
[3] P.N. Ross and M. Sattler, *J. Electrochem. Soc., 135* (1988) 1464.
[4] A.K. Shukla, A.M. Kannan, M.S. Hegde and J. Gopalakrishnan, *J. Power Sources, 35* (1991) 163.
[5] L. Swette, N. Kackley and S.A. McGatty, *J. Power Sources, 36* (1991) 323.
[6] T.R. Felthouse, P.B. Fraundorf, R.M. Friedman and C.L. Schosser, *J. Catal., 127* (1991) 393.
[7] A.M. Kannan, A.K. Shukla and S. Sathyanarayana, *J. Electroanal. Chem., 281* (1990) 339.
[8] J. Prakash, D. Tryk, W. Aldred and E. Yeager, Transition–metal oxide electrocatalysts for O_2 electrodes: The pyrochlores, in O.J. Murphy, S. Srinivasan and B.E. Conway (eds.), *Electrochemistry in Transition*, Plenum, New York, 1992.
[9] J. Prakash, D. Tryk and E. Yeager, *J. Power Sources, 29* (1990) 413.

[10] N.A. Vante, B. Schubert, H. Tributsch and A. Perrin, *J. Catal., 112* (1988) 384.
[11] H. Tamara, H. Yoneyama and Y. Matsumoto, in S. Trasatti (ed.), *Electrodes of Conductive Metallic Oxides*, Elsevier, New York, 1980.
[12] J.B. Goodenough, R. Manoharan and M. Paranthaman, *J. Am. Chem. Soc., 112* (1990) 2076.
[13] J.O'M. Bockris and T. Otagawa, *J. Phys. Chem., 87* (1983) 2960.
[14] R. Manoharan, M. Paranthaman and J.B. Goodenough, *Eur. J. Solid State Inorg. Chem., 26* (1989) 155.
[15] R.J. Bouchard and J.L. Gillson, *Mater. Res. Bull., 6* (1971) 669.
[16] Y. Shimizu, K. Uemura, H. Matsuda, N. Miura and N. Yamazoe, *J. Electrochem. Soc., 137* (1990) 3430.
[17] J.O'M. Bockris and T. Otagawa, *J. Electrochem. Soc., 131* (1984) 291.
[18] R. Manoharan and A.K. Shukla, *Electrochim. Acta, 30* (1985) 205.
[19] S.J. Schneider, J.L. Waring and R.E. Tressler, *J. Res. Nat. Bur. Stand., Sect. A, 69* (1965) 245.
[20] M.A. Subramanian, G. Aravamudan and G.V. Subba Rao, *Prog. Solid State Chem., 15* (1983) 55.
[21] H.S. Horowitz, J.M. Longo and J.T. Lewandowski, *Mater. Res. Bull., 16* (1981) 489.
[22] J.M. Longo, P.M. Raccah and J. Goodenough, *Mater. Res. Bull., 4* (1969) 191.
[23] W.D. Komer and D.J. Machin, *J. Less-Common Met., 61* (1978) 91.
[24] J.F. Vente and D.J.W. IJdo, *Mater. Res. Bull., 26* (1991) 1255.
[25] J.F. Vente, Iridium-oxide compounds, *Ph.D. Thesis*, University of Leiden, Netherlands, 1994.
[26] R.C. Currie, J.F. Vente, E. Frikkee and D.J.W. IJdo, *J. Solid State Chem.*, accepted for publication.
[27] F. Galasso and W. Darby, *Inorg. Chem., 4* (1965) 71.
[28] A.V. Powell, J.G. Gore and P.D. Battle, *J. Alloys Comp., 201* (1993) 73.
[29] E.M. Ramos, I. Alvarez, M.L. Veiga and C.Pico, *Mater. Res. Bull., 29* (1994) 881.
[30] M. Neubacher and H. Müller-Buschbaum, *Z. Anorg. Allg. Chem., 607* (1992) 124.
[31] F.J.J. Dijksma, J.F. Vente, E. Frikkee and D.J.W. IJdo, *Mater. Res. Bull., 28* (1993) 1145.
[32] L.J. van der Pauw, *Philips Res. Rep., 13* (1958) 1.
[33] J.J Yeh and I. Lindau, *At. Data Nucl. Data Tables, 32* (1985) 1–155.
[34] R. Holze, Impedanzmessungen an porösen Elektroden, *Ph.D. Thesis*, University of Bonn, Germany, 1983.
[35] M. Pourbaix, *Atlas of Electrochemical Equilibria in Aqueous Solutions*, National Association of Corrosion Engineers, TX, USA, 2nd edn., 1974.
[36] A.J. Bard, R. Parsons and J. Jordan, *Standard Potentials in Aqueous Solutions*, International Union of Pure and Applied Chemistry, New York, USA, 1985.
[37] A. Wattiaux, *Ph.D. Thesis*, University of Bordeaux, France, 1985.
[38] V.B. Lazarev and I.S. Shaplygin, *Russ. J. Inorg. Chem., 23* (1978) 291.
[39] J.M. Longo, P.M. Raccah and J.M. Goodenough, *J. Appl. Phys., 39* (1968) 1327.
[40] R.A. Beyerlein, H.S. Horowitz and J.M. Longo, *J. Solid State Chem., 72* (1988) 2.
[41] R. Kötz, H. Neff and S. Stucki, *J. Electrochem. Soc., 131* (1984) 72.
[42] G.K. Wertheim and H.J. Guggenheim, *Phys. Rev. B, 22* (1980) 4680.
[43] Perkin-Elmer Coorperation, *Handbook of X-ray Photoelectron Spectroscopy*, Eden Prairie, MI, 1977.
[44] G. Gökagaç and B.J. Kennedy, *J. Electroanal. Chem., 353* (1993) 71.
[45] K.S. Kim, W.E. Baitinger, J.W. Amy and N. Winograd, *J. Electron Spectrosc. Phenom., 5* (1974) 351.